Quaternion-based observer control for multirotor UAVs, an application to unactuated grasping

Diego Gandulfo, Alberto Varela, Pedro Castillo Garcia, Hernán Abaunza

Quaternion-based observer control for multirotor UAVs, an application to unactuated grasping

Diego Gandulfo[1,2], Alberto Varela[1,2], Pedro Castillo[1], and Hernán Abaunza [2,*]

***Abstract*— A novel approach for aerial drone control in object pickup tasks is presented. The methodology integrates quaternion-observer control to address the challenge of variable mass during object interaction. A specialized non-actuated gripper designed explicitly for aerial drones enhances their ability to grasp objects efficiently. Real-time tests validated the effectiveness and feasibility of the proposed solution. The experiments demonstrated the robustness and adaptability of quaternion-observer control in compensating for variable mass during object pickup tasks. Additionally, the practical utility of the non-conventional gripper design under real-world conditions emphasized its relevance in aerial manipulation scenarios.**

I. Introduction

In recent years, the utilization of Unmanned Aerial Vehicles (UAVs) has seen a significant rise not only for surveillance and data collection [1], but also for applications requiring interaction with the environment. Researchers have explored the use of UAVs, particularly quad-rotor drones, in areas such as obstacle avoidance, biomimetic landing [2], and object collection [3], [4]. UAVs have played a crucial role in technological research, influencing the evolution of various industries [5].

Commercial quadrotors, initially designed for photography and data collection using integrated cameras, are not inherently capable of supporting external payloads [6]. Consequently, for applications involving lifting objects, specialized or complex drones and high-cost grippers are often necessary, highlighting the complexity of both manual and autonomous use [7]. UAVs offer versatile solutions across different sectors, including industry, security, and production [8].

In [9], researchers and students implemented a gripper for a drone, enabling it to grasp surfaces during flight. Similarly, [10] utilized an actuated gripper to inspect electrical grid infrastructure. Actuated grippers offer advantages such as applied force, pose control, and task velocity, enhancing the drone's capabilities. In [11] dual arms were tested to evaluate the accuracy and behavior during physical procedures while flying.

However, actuated grippers introduce complexity, weight, and system dependence on sensors and commands. Grippers capable of providing feedback when closing with minimal energy consumption have been developed [12], offering ideal solutions for applications demanding high precision and controlled applied force. In [13] focuses on the new methods and technology applied to drones for physical interaction and contact inspection, using dual arms with multi-directional drones.

UAV interaction with ground objects has been a focus of research and innovation. While a drone can handle its weight during flights, introducing external objects or forces should be considered a disturbance. Addressing these disturbances during object pickup and reducing gripper weight, especially for commercial drones with limited load capacity, pose challenges.

In the realm of claw drones, noteworthy projects like "EagleClaw" [2] and origami-inspired arm drones [3] have emerged. The "EagleClaw" features a robust claw with impressive payload capacity, suitable for heavy loading and transport tasks in industrial environments. Origami-inspired arm drones, agile and precise in object manipulation, stand out for applications like garbage collection. There is a long reach arm manipulator that enhances maneuverability, adaptability in confined spaces, and a design that minimizes potential damage during interactions[14].

Disturbances in drones are commonly compensated using Disturbance-Observer-Based Control [15]. Various approaches exist, such as Equivalent Input Disturbance (EID), Extended State Observer (ESO), Generalized Proportional Integral Observer (GPIO), Linear/Nonlinear Disturbance Observer ((L/N)DOB), and others [15]. An implmentation of an Unknown Disturbance Estimator (UDE) has been designed for quadrotors in [16]. Recent research by [17] introduces a backstepping disturbance observer-based control (DOBC) for trajectory tracking of multirotor UAVs, [18] proposes a disturbance observer-based (DOB) control scheme tailored for small UAVs, characterized by nonlinear dynamics and uncertainties. The approach integrates transient performance design to ensure both steady-state and transient observation performance.

The goal of this paper is to implement an observer and a gripper, enabling a drone to autonomously navigate to an object, perform pickup, and transport it to a destination point while considering mass perturbations. For the pickup method, a non-conventional, non-actuated gripper is designed, scalable to any drone.

The structure of the paper is as follows. Section II provides the quadrotor modelling and control. Section III outlines the implemented observer approach, while Section IV introduces the gripper design and development. Section V details the tests and results. Finally, Section VI offers discussions on this work and outlines future steps.

[1] Université de Technologie de Compiègne, CNRS, Heudiasyc (Heuristics and Diagnosis of Complex Systems), CS 60319 - 60203 Compiegne Cedex, France. castillo@hds.utc.fr

[2] Tecnológico de Monterrey, Escuela de Ingeniería y Ciencias, Av. General Ramón Corona 2514, 45201 Zapopan, Jalisco, México. (A01639623,A01721564,habaunza)@tec.mx

[*] Corresponding Author

II. Quadrotor Quaternion Model and Control

A. Quadrotor Quaternion Dynamic Model

Consider a symmetrical quadrotor as depicted in Figure 1. According to blade element theory, each rotor $i : [1, \cdots, 4]$ generates a force $f_i := C_T \rho A_p r^2 \omega_i^2$ and a torque $\tau_i := C_Q \rho A_p r^3 \omega_i^2$ from its angular velocity ω_i, also dependent on the air density ρ, the rotating plate area A_p, the propeller's radius r, and aerodynamic coefficients C_T and C_Q [19].

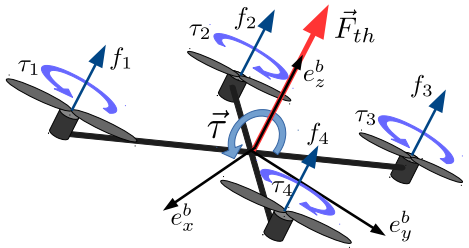

Fig. 1: Quadrotor total force $\vec{F}_{th}$ and torque $\vec{\tau}$ as illustrated in [19]

Hence, the thrust force F_{th} that acts vertically in the body reference frame can be computed as

$$\vec{F}_{th} := \begin{bmatrix} 0 & 0 & F_{th} \end{bmatrix}^T = \begin{bmatrix} 0 & 0 & \sum_{i=1}^{4} f_i \end{bmatrix}^T, \quad (1)$$

similarly, the total torque vector, acting in the body reference frame can be described as

$$\vec{\tau} := \begin{bmatrix} \tau_x \\ \tau_y \\ \tau_z \end{bmatrix} = \begin{bmatrix} (-f_1 - f_2 + f_3 + f_4) l \cos(\pi/4) \\ (-f_1 + f_2 + f_3 - f_4) l \cos(\pi/4) \\ \sum_{i=1}^{4} \tau_i \end{bmatrix}. \quad (2)$$

Where l represents the drone's arm length, which extends from the center of mass to each motor.

Define the quadrotor state as $X := [\vec{p}\ \dot{\vec{p}}\ \boldsymbol{q}\ \vec{\Omega}]^T$ where $\vec{p} \in \mathbb{R}^3$ denotes the drone's position in the inertial frame, $\dot{\vec{p}}$ represents its velocity, $\boldsymbol{q} := q_0 + [q_1\ q_2\ q_3]^T \in \mathbb{H}$ defines its orientation represented as a unit quaternion and $\vec{\Omega} := [\omega_x\ \omega_y\ \omega_z]^T$ is its rotational velocity on the body frame. Then, from (1) and (2), the quadrotor dynamic model can be expressed as

$$\dot{X} = \frac{d}{dt} \begin{bmatrix} \vec{p} \\ \dot{\vec{p}} \\ \boldsymbol{q} \\ \vec{\Omega} \end{bmatrix} = \begin{bmatrix} \dot{\vec{p}} \\ \boldsymbol{q} \otimes \frac{\vec{F}_{th}}{m} \otimes \boldsymbol{q} + \vec{g} + \vec{\gamma} \\ \frac{1}{2} \boldsymbol{q} \otimes \vec{\Omega} \\ J^{-1}(\vec{\tau} - \vec{\Omega} \times J\vec{\Omega}) \end{bmatrix}, \quad (3)$$

where $\otimes$ represents a quaternion product, m and J are the drone's mass and inertia matrix respectively, $\vec{g} := [0\ \ 0\ -9.81]^T$, is the gravitational acceleration vector, and $\vec{\gamma} \in \mathbb{R}^3$ symbolizes an unknown disturbance vector.

B. Quadrotor underactuation problem

Notice that (3) is an underactuated dynamic system consisting on 6 degrees of freedom (3 rotational and 3 translational) and four control inputs (one total thrust force F_{th} and three torques $\vec{\tau} \in \mathbb{R}^3$). However, the rotational subsystem is indeed fully actuated, and can be written as

$$\dot{X}_r = \begin{bmatrix} \frac{1}{2} \boldsymbol{q} \otimes \vec{\Omega} \\ J^{-1}(\vec{\tau} - \vec{\Omega} \times J\vec{\Omega}) \end{bmatrix}, \quad (4)$$

Following [19] and [20], (4) can be stabilized to a desired unit quaternion $\boldsymbol{q}_d$ by applying a state feedback controller using a quaternion logarithm, resulting in

$$\vec{\tau} = -2K_{pr} \ln(\boldsymbol{q}_d^* \otimes \boldsymbol{q}) - K_{dr} \vec{\Omega}, \quad (5)$$

where $\boldsymbol{q}_d^*$ is the conjugate quaternion of $\boldsymbol{q}_d$, K_{pr} and K_{dr} are positive constant diagonal matrices containing proportional and derivative gains respecively.

Therefore, if (5) ensures that $\boldsymbol{q} \approx \boldsymbol{q}_d$, then, from (3) the traslational subsystem can be written as

$$\dot{X}_t = \begin{bmatrix} \dot{\vec{p}} \\ \boldsymbol{q} \otimes \frac{\vec{F}_{th}}{m} \otimes \boldsymbol{q} + \vec{g} + \vec{\gamma} \end{bmatrix} \approx \begin{bmatrix} \dot{\vec{p}} \\ \boldsymbol{q}_d \otimes \frac{\vec{F}_{th}}{m} \otimes \boldsymbol{q}_d + \vec{g} + \vec{\gamma} \end{bmatrix}. \quad (6)$$

Following the methodology presented in [19]-[21], a virtual control force $\vec{F}_u \in \mathbb{R}^3$ can be defined as $\vec{F}_u := \boldsymbol{q}_d \otimes \frac{\vec{F}_{th}}{m} \otimes \boldsymbol{q}_d + \vec{g}$ such that (6) becomes

$$\dot{X}_t \approx \begin{bmatrix} \dot{\vec{p}} \\ \vec{F}_u + \vec{\gamma} \end{bmatrix} = \begin{bmatrix} 0^{3\times3} & I^{3\times3} \\ 0^{3\times3} & 0^{3\times3} \end{bmatrix} X_t + \begin{bmatrix} 0^{3\times3} \\ I^{3\times3} \end{bmatrix} \left[\vec{F}_u + \vec{\gamma} \right], \quad (7)$$

where $0^{3\times3}$ and $I^{3\times3}$ respectively symbolize 3×3 zeroes and identity matrices. Notice that (7) can be seen as a linear fully actuated representation of the traslational dynamics.

Since $\vec{F}_u$ can be designed by following any control strategy, including a compensation for the disturbance $\vec{\gamma}$, then the desired quaternion $\boldsymbol{q}_d$ is computed as $\boldsymbol{q}_d := \boldsymbol{q}_{xy} \otimes \boldsymbol{q}_z$, where $\boldsymbol{q}_{xy}$ represents the shortest rotation that aligns the thrust vector $\vec{F}_{th}$ towards the control force $\vec{F}_u$ [20], [21] and is defined by following the Euler-Rodrigues formula as

$$\boldsymbol{q}_{xy} := \pm \sqrt{\frac{1 + \frac{\vec{F}_u}{\|\vec{F}_u\|} \cdot \begin{bmatrix} 0 \\ 0 \\ 1 \end{bmatrix}}{2}} + \frac{\frac{\vec{F}_u}{\|\vec{F}_u\|} \times \begin{bmatrix} 0 \\ 0 \\ 1 \end{bmatrix}}{\left\| \frac{\vec{F}_u}{\|\vec{F}_u\|} \times \begin{bmatrix} 0 \\ 0 \\ 1 \end{bmatrix} \right\|} \sqrt{\frac{1 - \frac{\vec{F}_u}{\|\vec{F}_u\|} \cdot \begin{bmatrix} 0 \\ 0 \\ 1 \end{bmatrix}}{2}}, \quad (8)$$

while $\boldsymbol{q}_z$ defines an aditional desired rotation over the z axis (yaw rotation), and is computed as

$$\boldsymbol{q}_z = \cos \frac{\psi_d}{2} + [0\ 0\ 1]^T \sin \frac{\psi_d}{2}, \quad (9)$$

where ψ_d represents the desired yaw rotation

C. State Feedback Controller

For comparison purposes, a simple state feedback (proportional-derivative (PD)) was implemented to control the quadrotor traslational dynamics. Defining $\vec{F}_u$ in this manner, and neglecting the unknown disturbance $\vec{\gamma} \approx [0\ \ 0\ \ 0]^T$ yields

$$\vec{F}_u = -K_{pt}(\vec{p} - \vec{p}_d) - K_{dt}(\dot{\vec{p}} - \dot{\vec{p}}_d) - m\vec{g}, \quad (10)$$

where K_{pt} and K_{dt} are positive constant diagonal matrices and $\vec{p}_d \in \mathbb{R}^3$ represents a desired position.

The control inputs are then defined for system (3), computing $\boldsymbol{q}_d$ by introducing (10) into (8) and asigning any yaw angle reference ψ_d for (9), and using (5) to track the

desired attitude $\boldsymbol{q}_d$. The thrust force is then computed as $F_{th} = ||\vec{F}_u||$.

III. Uncertainty and Disturbance Estimator

Controller (10) does not consider any disturbance in the system and is dependent on accurate and constant weight parameters. However, in reality the drone can be affected by many perturbations such as wind, or in the case of the topic of this work, weight changes when grasping an object. Therefore, from (7), a virtual disturbed linear translational system can be considered as

$$\dot{X}_t \approx A_t X_t + B_t \left[\vec{F}_u + \vec{\gamma}\right], \tag{11}$$

where $A_t := \begin{bmatrix} 0^{3\times3} & I^{3\times3} \\ 0^{3\times3} & 0^{3\times3} \end{bmatrix}$ and $B_T := \begin{bmatrix} 0^{3\times3} \\ I^{3\times3} \end{bmatrix}$.

An uni-formal perturbation is here assumed so it doesn't affect the rotational system.

A. Perturbation controller

The control strategy that will be applied consists on estimating the disturbance by means of an observer approach known as *Unknown Disturbance Estimator* (UDE) [16]. Here, an estimation $\hat{\vec{\gamma}}(t)$ is designed such that $\hat{\vec{\gamma}}(t) \to \vec{\gamma}(t)$ and then added to controller (10) as

$$\vec{F}_u(t) = -K_{pt}(\vec{p} - \vec{p}_d) - K_{dt}(\dot{\vec{p}} - \dot{\vec{p}}_d) - m(\vec{g} + \hat{\vec{\gamma}}(t)). \tag{12}$$

From 11, the reduced-order observer following the UDE design procedure proposed by [22] and [16] yields

$$\gamma(t) = B_t^+[\dot{X}_t(t) - A_t X_t(t) - B_t \vec{F}_u(t)], \tag{13}$$

being $B_t^+ = (B_t^T B_t)^{-1} B_t^T$ the pseudoinverse of B_t and this determines that $B_t^+ = [0\ m]$, since (13) cannot be directly computed, the following estimation is proposed:

$$\dot{\hat{\vec{\gamma}}}(t) = -\Gamma\hat{\vec{\gamma}}(t) + \Gamma B_t^+ \left[\dot{X}_t(t) - AX_t(t) - B_t\vec{F}_u(t)\right], \tag{14}$$

where $\Gamma \triangleq \mathrm{diag}(\Gamma_1, \Gamma_2, ..., \Gamma_6)$, being $\Gamma_j > 0, j : [1, \cdots, 6]$ and for avoiding the term $\dot{X}_t(t)$ the next change of variable is applied

$$\hat{\xi}(t) = \hat{\vec{\gamma}}(t) + \Gamma B_t^+ X_t(t). \tag{15}$$

Taking the derivative of equation (17) and applying equations (5) and (16) results in the derivation of the reduced-order observer mentioned below:

$$\begin{cases} \dot{\hat{\xi}}(t) = -\Gamma\hat{\xi}(t) - \left(\Gamma^2 B_t^+ + \Gamma B_t^+ A\right) X_t(t) - \Gamma\vec{F}_u(t), \\ \hat{\vec{\gamma}}(t) = \hat{\xi}(t) + \Gamma B_t^+ X_t(t), \qquad \xi(0) = -\Gamma B_t^+ X_t(0). \end{cases} \tag{16}$$

The control strategy is then completed by mumerically computing $\hat{\xi}(t) = \int \dot{\hat{\xi}}(t)dt$, and then introducing system (16) into (12).

IV. Gripper Development

The final design of the gripper was chosen by testing two types of grippers, and the most suitable one for the desired purpose was selected. The first option, based on [23], was redesigned for testing purposes, as depicted in Fig. 2. This gripper, originally designed for an actuated mechanism, had its actuator replaced with a newly designed gripper mechanism, shown in Fig. 3. After conducting physical tests, the first gripper was replaced by the second option due to its lower pressure requirement for closure and object grasping, which was approximately 20 Newtons.

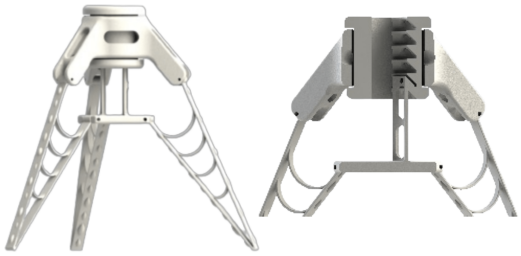

Fig. 2: First Gripper Option

The second gripper option was derived from the *Mantis Claw* designed by Ben Kardoosh [24], being adapted to meet the specified requirements while enhancing several characteristics. This entailed a reduction in the number of parts, simplification of assembly, and minimization of weight to achieve improved performance.

Fig. 3: Gripper in closed position while flying

Fig. 4: Gripper in open position while being in touch with the object

This gripper was selected for the task based on its high effectiveness in the 3D prototype test. The object is grabbed without the use of external forces, and closing the gripper only relies on gravity and the weight of the object itself, as illustrated in Fig. 3. Mechanical restrictions are employed to prevent the object from falling. Subsequently, the weight of the drone is measured, as shown in Fig. 7, and through lifting tests, it was determined that the gripper can support up to 300

grams without deterioration. The model was not physically tested beyond that weight limit, focusing on objects lighter than the specified weight.

By applying Finite Element Analysis (FEA) and using Von Mises theory, is possible to predict the plastic deformation of the most crucial parts of the gripper.

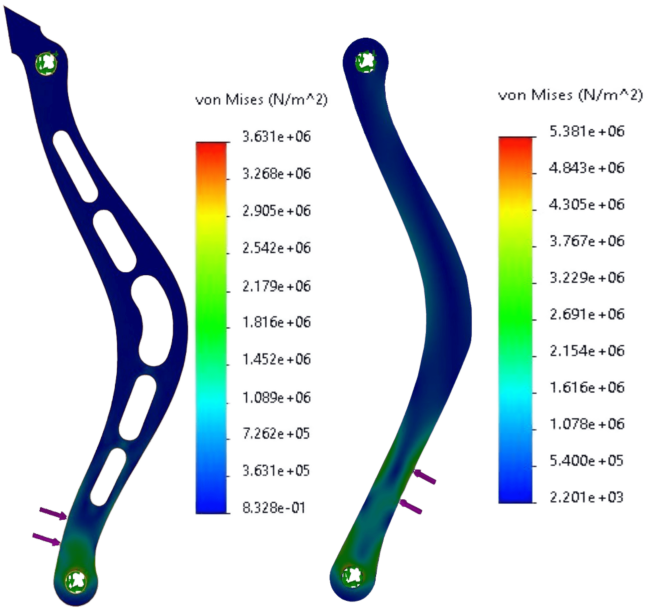

Fig. 5: Finite Element Analysis applied to the gripper's arm

The material applied to the parts is ABS, the same that is used for the prototype, which has a Young's modulus of $2 \times 10^9\,\mathrm{N/m^2}$ and a yield strength of $3.2 \times 10^7\,\mathrm{N/m^2}$ [25]. These are the references and limits while using FEA. As in Fig. 5-6, the plastic deformation of any part will be less than $1.672 \times 10^7\,\mathrm{N/m^2}$.

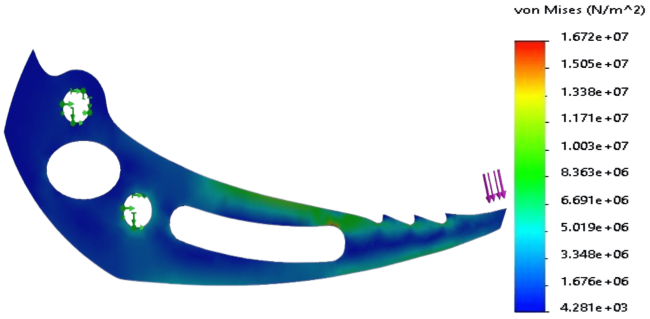

Fig. 6: Finite Element Analysis applied to the gripper's claw

Note that the mesh employed for each component consisted of 16 Jacobian points and mesh quality characterized by high-order quadratic elements. The purple arrows in each part represent a stress of $19.208\,\mathrm{N/m^2}$, equivalent to 200 grams of weight applied to each claw of gripper-1 kg of weight is equal to $95.64\,\mathrm{N/m^2}$ divided by the 5 claws. The green arrows represent a fixed geometry. The Von Mises range for each part spans from $8.328 \times 10^1\,\mathrm{N/m^2}$ to $1.672 \times 10^7\,\mathrm{N/m^2}$. Comparing these stress values with the ABS Yield strength requirement of $3.2 \times 10^7\,\mathrm{N/m^2}$, it is evident that the gripper is well within the safe stress limits carrying objects less than 1 kilogram of weight. If necessary, it is possible to adjust the size and material of the gripper to decrease the undergoing plastic deformation.

With less than 40 grams of weight (as seen in Figure 7), the gripper is ready for experimental tests. Now, considering the maximum lifting weight of our drone, 200 grams, it is possible to carry up to 160 grams approximately.

Fig. 7: Weight of the scaled gripper for the quadrotor used

An additional attribute of this gripper is its scalability, allowing it to accommodate to various types of drones. Moreover, it can be crafted from alternative materials to optimize load capacity. The underlying concept is to address diverse tasks involving object retrieval, irrespective of size or weight. This is achieved by developing a model capable of adjusting the base that attaches to the drone, thereby integrating the gripper seamlessly with the drone system. Repository: `https://github.com/AlbertoVC20/Gripper-QuaternionControl/tree/main`.

V. Tests and Results

A. *Fl-AIR - Framework libre AIR*

For trajectory and control testing, Fl-AIR [26] was used to simulate all our changes. Fl-Air is a framework written in C++ that aims at helping the development of applications for robots, and more specially for UAVs. This platform is free to use, where the codes are simulated before testing with the prototype, saving this way time and resources, Fig. 8.

Fig. 8: Fl-Air demonstration using the integrated simulator

Using Fl-Air to simulate our code and trajectories was a huge advantage and time-saving. Then proceed to test it using the Drone Parrot 2.

B. Drone Parrot A.R.Drone 2.0

For our project tests, the Parrot A.R. Drone 2.0 was used, which has a maximum load capacity of approximately 200 grams. As in Fig. 9, the gripper was mounted to the drone in the inferior part, and using some security mattresses, the drone was elevated for which the gripper can hang without touching the ground. In this exact same position, the drone will return after picking up the object, and land safely in the same spot.

Fig. 9: Drone Parrot A.R. Drone 2.0 with the designed gripper mounted

The quadrotor position and translational velocity was estimated using an *OptiTrack* [27] motion capture system, while its orientation quaternion and angular velocity was measured using the internal Inertial Measurement Unit (IMU) and a Kalman Filter.

C. Desired Trajectory

To generate the desired trajectory $\vec{p}_d(t)$, the first step involved considering the initial position of the drone and the position of the object. Based on these two points, a line was generated using the equation of a straight line but with a safety margin added in the z-axis. Once this was completed, the drone proceeded to linearly decrease its position along the z-axis until reaching the position of the object. Subsequently, it increased its position again until returning to its original z-axis position. Following this, using the equation of a straight line once more, the drone navigated to the landing position along the x-axis without altering its z-axis value. Finally, it descended along the z-axis to its landing position.

D. Final Results

Two tests were made, one using only a state-feedback quaternion control as in [20], and the other one implementing the observer.The experimental outcomes are presented below, delineating the focus on evaluating flight performance during object pickup with the application of the quaternion-observer control. A comparative analysis is conducted, contrasting these results with the drone's behavior and outcomes during flights conducted without the observer.

Application of the quaternion-observer control during object pickup demonstrated a discernible improvement in flight dynamics. The observer effectively compensated for variable mass, resulting in enhanced stability and more precise object grasping. Comparative analyses revealed that flights with the observer exhibited superior trajectory adherence, underscoring the control strategy's efficacy in optimizing flight paths. In contrast, flights without the observer displayed heightened sensitivity to variations in object mass, leading to less predictable flight behavior. These findings emphasize the tangible benefits of incorporating quaternion-observer control for enhancing the reliability and precision of aerial drones during object manipulation tasks.

A comparison between the tests with and without observer is available at: `https://youtu.be/wrHi-607hw8`.

For this application, the displacement behavior analysis is more significant on the z axis, because it is where the external force is being mainly applied, in this case, the payload weight. Therefore, the effect on the x and y axes is minimal.

Observe from Figure 10 that at no point can the quadrotor reach the reference, as it cannot even compensate for the gripper's weight. The most noticeable change occurs when the gripper picks up the object at around time $t = 30s$, at which point the difference between the position and the reference increases significantly.

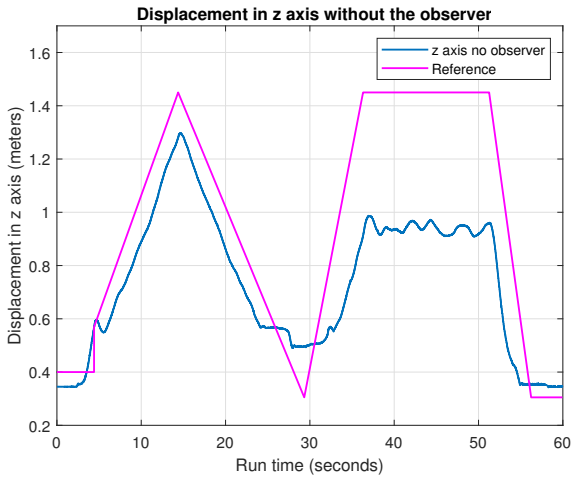

Fig. 10: z position without applying the observer

Remark from the beginning of Figure 11 how the observer compensates for the gripper's weight, where initially there is a small difference between the drone position and its reference, but it is almost completely eliminated after a few seconds. When the object is picked up at $t = 34.4$, a slight discrepancy between the position and the reference can be observed, and when the drone needs to maintain its position in z from $t = 41.4$ to $t = 56.4$, there are small oscillations that decrease over time. Lastly, when descending, it can be noticed that the position error is practically null.

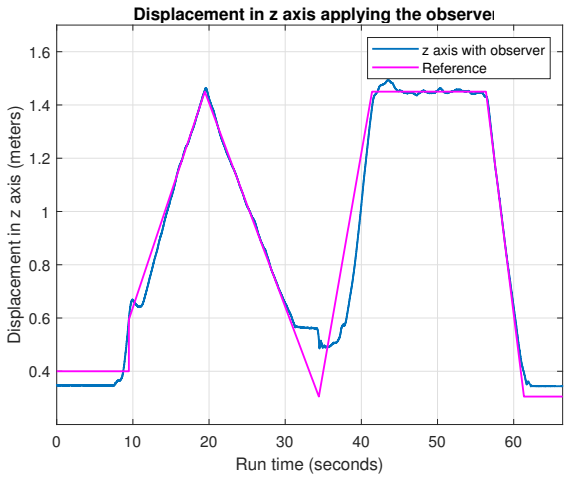

Fig. 11: z position applying the observer

Observe in Figure 12 how the drone follows the reference at all times. However, in the time interval from $t = 14.4$ to $t = 36.4$, some oscillations can be noticed due to the effects of the gripper.

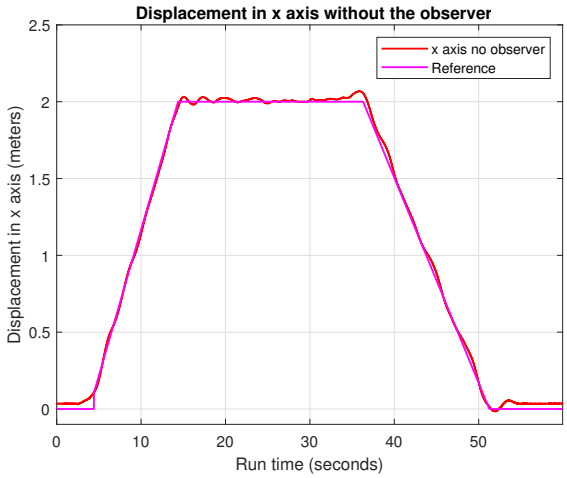

Fig. 12: x position without applying the observer

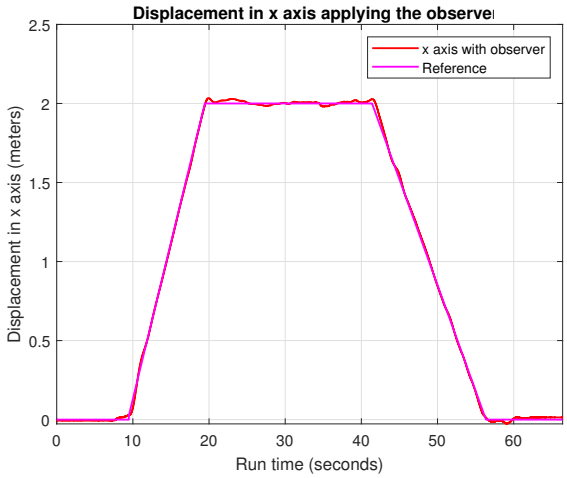

Fig. 13: x position applying the observer

Remark in Figure 13, it is observed how the drone follows the reference almost perfectly regardless of the unknown disturbance. The most notable difference from 12 is that when it has to hold its position, the oscillations are practically nonexistent thanks to the observer.

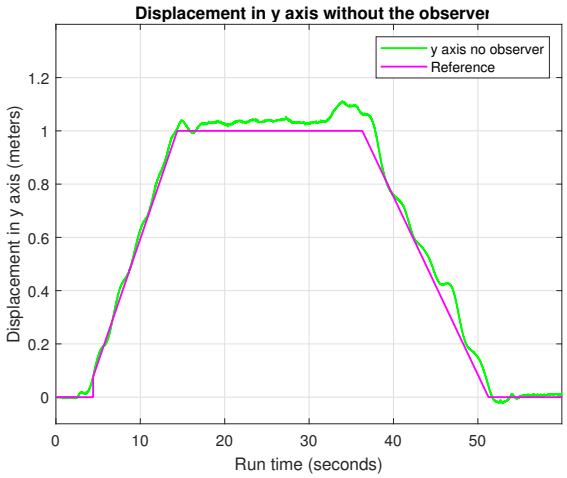

Fig. 14: y position without applying the observer

Figure 14 shows how, initially, when there is no payload, as the position value increases, the drone is capable of following the reference with some minor difference. However, in the following two stages, when the object is grasped, the increased disturbance results in a considerable error.

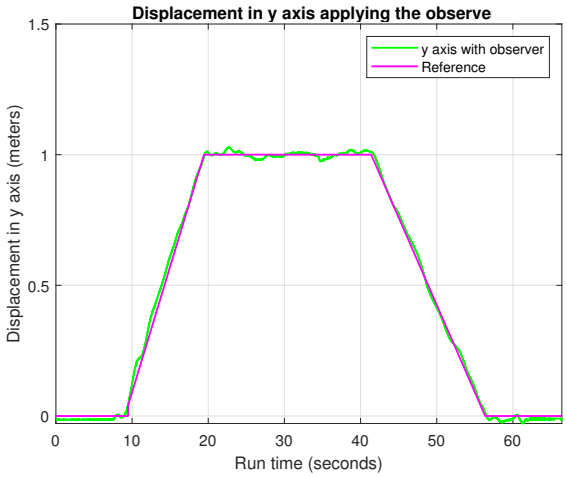

Fig. 15: y position applying the observer

As indicated by Figure 15, unlike Figure 14, it is evident that the drone can successfully track the reference. Only minor oscillations can be observed in the position holding part, but they are quite insignificant and much smaller compared to the test conducted without the observer.

Analyzing these results, it can be observed how the drone's behavior in all three axes is superior when using the observer. The most noticeable difference lies in the z-axis after object collection. As seen in the graphs and video, once the object is collected, the drone without the observer is unable to reach

the reference by a considerably large distance. In contrast, the drone using the observer successfully reaches the reference in the z-axis, albeit with some oscillations. As for the remaining axes, x and y, slight improvements can be observed when using the observer, especially in reducing oscillations.

VI. Conclusions and future perspectives

In this paper, the quaternion-observer control was successfully applied along with a UDE-based controller, providing a robust response to perturbations. Additionally, a lightweight gripper was designed, focusing on mechanical pickup rather than an actuated mechanism. This design choice enhances the object retrieval process and facilitates various applications, including increased maximum lift capacity, lower center of mass, and scalability of the gripper.

As demonstrated in the results, the drone's response varies significantly when the observer is applied compared to when it is not, particularly when subjected to significant perturbations, such as the addition of weight, as observed in this case.

Acknowledgments

The authors want to express gratitude to the ROBOTEX project for providing the equipment needed for this work, and to Guillaume Sanahuja, Thierry Monglon, and Vinicius Pacheco for their technical support.

References

[1] V. S. Kumar, M. Sakthivel, D. A. Karras, S. K. Gupta, S. M. P. Gangadharan, and B. Haralayya, "Drone surveillance in flood affected areas using firefly algorithm," in *2022 International Conference on Knowledge Engineering and Communication Systems (ICKES)*, pp. 1–5, IEEE, 2022.

[2] W. R. Roderick, M. R. Cutkosky, and D. Lentink, "Bird-inspired dynamic grasping and perching in arboreal environments," *Science Robotics*, vol. 6, no. 61, p. eabj7562, 2021.

[3] S.-J. Kim, D.-Y. Lee, G.-P. Jung, and K.-J. Cho, "An origami-inspired, self-locking robotic arm that can be folded flat," *Science Robotics*, vol. 3, no. 16, p. eaar2915, 2018.

[4] J. Thomas, J. Polin, K. Sreenath, and V. Kumar, "Avian-inspired grasping for quadrotor micro uavs," in *International Design Engineering Technical Conferences and Computers and Information in Engineering Conference*, vol. 55935, p. V06AT07A014, American Society of Mechanical Engineers, 2013.

[5] R. Briefs, "How drones will impact society: From fighting war to forecasting weather, uavs change everything," *Insights, CB*, vol. 7, 2020.

[6] J. S. Patel, C. Al-Ameri, F. Fioranelli, and D. Anderson, "Multi-time frequency analysis and classification of a micro-drone carrying payloads using multistatic radar," *The Journal of Engineering*, vol. 2019, no. 20, pp. 7047–7051, 2019.

[7] M. Hassanalian and A. Abdelkefi, "Classifications, applications, and design challenges of drones: A review," *Progress in Aerospace Sciences*, vol. 91, pp. 99–131, 2017.

[8] M. Ayamga, S. Akaba, and A. A. Nyaaba, "Multifaceted applicability of drones: A review," *Technological Forecasting and Social Change*, vol. 167, p. 120677, 2021.

[9] H. Zhang, E. Lerner, B. Cheng, and J. Zhao, "Compliant bistable grippers enable passive perching for micro aerial vehicles," *IEEE/ASME Transactions on Mechatronics*, vol. 26, no. 5, pp. 2316–2326, 2020.

[10] O. B. Schofield, K. H. Lorenzen, and E. Ebeid, "Cloud to cable: A drone framework for autonomous power line inspection," in *2020 23rd Euromicro Conference on Digital System Design (DSD)*, pp. 503–509, IEEE, 2020.

[11] A. Suarez, P. J. Sanchez-Cuevas, G. Heredia, and A. Ollero, "Aerial physical interaction in grabbing conditions with lightweight and compliant dual arms," *Applied Sciences*, vol. 10, no. 24, 2020.

[12] M. Lieret, J. Lukas, M. Nikol, and J. Franke, "A lightweight, low-cost and self-diagnosing mechatronic jaw gripper for the aerial picking with unmanned aerial vehicles," *Procedia Manufacturing*, vol. 51, pp. 424–430, 2020.

[13] A. Ollero, G. Heredia, A. Franchi, G. Antonelli, K. Kondak, A. Sanfeliu, A. Viguria, J. R. Martinez-de Dios, F. Pierri, J. Cortes, A. Santamaria-Navarro, M. A. Trujillo Soto, R. Balachandran, J. Andrade-Cetto, and A. Rodriguez, "The aeroarms project: Aerial robots with advanced manipulation capabilities for inspection and maintenance," *IEEE Robotics & Automation Magazine*, vol. 25, no. 4, pp. 12–23, 2018.

[14] A. Suarez, P. Sanchez-Cuevas, M. Fernandez, M. Perez, G. Heredia, and A. Ollero, "Lightweight and compliant long reach aerial manipulator for inspection operations," in *2018 IEEE/RSJ International Conference on Intelligent Robots and Systems (IROS)*, pp. 6746–6752, 2018.

[15] W.-H. Chen, J. Yang, L. Guo, and S. Li, "Disturbance-observer-based control and related methods—an overview," *IEEE Transactions on industrial electronics*, vol. 63, no. 2, pp. 1083–1095, 2015.

[16] A. Castillo, R. Sanz, P. Garcia, and P. Albertos, "Robust design of the uncertainty and disturbance estimator," *IFAC-PapersOnLine*, vol. 50, no. 1, pp. 8262–8267, 2017.

[17] A. Moeini, A. F. Lynch, and Q. Zhao, "A backstepping disturbance observer control for multirotor uavs: Theory and experiment," *International Journal of Control*, vol. 95, no. 9, pp. 2364–2378, 2022.

[18] J. Chen, R. Sun, and B. Zhu, "Disturbance observer-based control for small nonlinear uav systems with transient performance constraint," *Aerospace Science and Technology*, vol. 105, p. 106028, 2020.

[19] H. Abaunza, *Robust tracking of dynamic targets with aerial vehicles using quaternion-based techniques*. PhD thesis, Université de Technologie de Compiègne, 2019.

[20] J. Carino, H. Abaunza, and P. Castillo, "Quadrotor quaternion control," in *2015 International Conference on Unmanned Aircraft Systems (ICUAS)*, pp. 825–831, IEEE, 2015.

[21] J. Cariño, H. Abaunza, and P. Castillo, "A fully-actuated quadcopter representation using quaternions," *International Journal of Control*, pp. 1–23, 2022.

[22] Q.-C. Zhong and D. Rees, "Control of uncertain lti systems based on an uncertainty and disturbance estimator," *J. Dyn. Sys., Meas., Control*, vol. 126, no. 4, pp. 905–910, 2004.

[23] Thingiverse, "Load and wind aware routing of delivery drones," *https://www.thingiverse.com/thing:4269401*, 2023.

[24] T. Mogg, "The 'mantis drone claw' turns any quadcopter into a high-stakes arcade crane game," *Digital Trends*, 2015.

[25] Ensinger, "Tecaran abs grey product specifications," *https://www.ensingerplastics.com/es-br/semielaborados/plastico/tecaran-abs-grey*, 2023.

[26] G. Sanahuja, "Fl-air (framework libre air)," *https://devel.hds.utc.fr/software/flair*, 2023.

[27] OptiTrack, "Motion capture systems," *https://optitrack.com*, 2023.